Fluorescence Correlation Spectroscopy Analysis of Diffusion in a Laser Gradient Field: A Numerical Approach

Fanbo Meng[†] and Hui Ma*[,†,‡]

Department of Physics, Tsinghua University, Beijing 100084, China, and Graduate School at Shenzhen, Tsinghua University, Shenzhen 518055, China

Received: November 7, 2004; In Final Form: January 20, 2005

Fluorescence correlation spectroscopy (FCS) is widely used in biological systems. When the laser is intense enough, such as in two-photon experiments, the trapping force due to the laser gradient field can change the diffusion behavior of the fluorescent particles and induce error in the FCS measurements. Previous studies on biased FCS are qualitative. In this article, a numerical approach is proposed to treat the problem quantitatively. By assumption of a "spherical symmetry", biased FCS curves can be calculated numerically and fitted to the experimental data to retrieve the unbiased particle number, diffusion time, and polarizability of the fluorescent particles as well as the strength of the gradient field. It has been proven using simulated FCS data that the discrepancy caused by the spherical symmetry approximation is independent of the gradient field strength; therefore it can be eliminated by a calibration.

1. Introduction

Fluorescence correlation spectroscopy (FCS) is a sensitive technique for in vivo investigations of a wide variety of chemical and physical processes.[1−5] In FCS, fluorescence fluctuation spectra from sparse fluorescent particles diffusing through the focal spot of an excitation laser are recorded. Autocorrelation curves of the spectra are then calculated and fitted to a theoretical model to obtain parameters that affect the fluorescence fluctuation, such as particle concentration, diffusion mobility, etc. Because of its high sensitivity, low invasion, and the prospect for real-time in vivo measurements, FCS has been gaining popularity in biological applications.

In the current FCS theory, perturbation to diffusion dynamics by the excitation laser is not considered. Laser intensity does not appear in the normalized FCS formula. However, the electric field due to the excitation laser will interact with the electric dipole of the molecules and apply a gradient force on the molecules.[6−9] When the laser is tightly focused by a high numerical aperture objective and its intensity is high, the gradient force may become strong enough to alter the diffusion dynamics and manifest itself in biased photon statistics.[10]

It was observed that the retrieved diffusion coefficients of rhodamine 6G (R6G) molecules by FCS experiments did depend on the intensity of the excitation laser.[11] The diffusion time for the molecules to travel across the focal spot increased linearly with the power of the excitation laser. However, a more rapid growth in the fitted diffusion time was observed in our previous experiments using microspheres and also in simulations.[12] Chirico et al. discovered the power dependence of the local concentration and confirmed the two different trends in the diffusion times of R6G and microspheres.[13] An approximate approach derived by our group[14] predicted a growth curve similar to an exponential function.

The previous attempts to interpret biased FCS experiments were qualitative. In this article, a quantitative numerical approach is presented to retrieve more details on biased diffusion dynamics of the molecules. FCS curves in a laser gradient field are calculated numerically for spherically symmetric systems and are fitted to FCS data. Unlike the previous method, which gives approximately the biased local concentration and diffusion time, this approach retrieves directly the unbiased parameters such as the actual concentration of the solution and the diffusion coefficient of the particles. Although the assumption of a spherically symmetric system is far from the real situations encountered in experiments, it results in only systematic errors that can be factored out by calibrations.

2. Theoretical Framework

An FCS function can be written as[3,4]

$$G(\tau) = \frac{\int\int W(\vec{r})\langle \delta C(\vec{r},t)\delta C(\vec{r}',t+\tau)\rangle W(\vec{r}')\, \mathrm{d}^3\vec{r}\, \mathrm{d}^3\vec{r}'}{(\int W(\vec{r})\langle C(\vec{r},t)\rangle\, \mathrm{d}^3\vec{r})^2} = \frac{\int\int W(\vec{r})C(\vec{r})P(\vec{r},\vec{r}',\tau)W(\vec{r}')\, \mathrm{d}^3\vec{r}\, \mathrm{d}^3\vec{r}'}{(\int W(\vec{r})C(\vec{r})\, \mathrm{d}^3\vec{r})^2} \quad (1)$$

where $C(\vec{r},t)$ is the concentration of fluorescent particles, $C(\vec{r}) = \langle C(\vec{r},t)\rangle$ is the equilibrium concentration, $\langle\cdots\rangle$ means the temporal average, $\delta C(\vec{r},t) = C(\vec{r},t) - C(\vec{r})$ is the fluorescence fluctuation, $P(\vec{r},\vec{r}',\tau)$ is called the "propagator",[15] which represents the possibility that a particle starting from $\vec{r}$ diffuses to $\vec{r}'$ after a time period τ, and $W(\vec{r})$ is the normalized intensity distribution of the excitation laser, which satisfies $W(0) = 1$ and is often chosen as a three-dimensional (3D) Gaussian function in FCS studies

$$W(\rho,z) = \exp\left(-\frac{2\rho^2}{{w_0}^2} - \frac{2z^2}{{z_0}^2}\right) \quad (2)$$

* Author to whom correspondence should be addressed. E-mail: mahui@tsinghua.edu.cn.
[†] Tsinghua University, Beijing.
[‡] Tsinghua University, Shenzhen.

10.1021/jp044898g CCC: $30.25
Published on Web 02/24/2005

where w_0 and z_0 are the radial and axial beam waists, respectively. The optical-transfer function of the objective−pinhole combination is chosen as constant in this work, because it was proven that the pinhole had little effect on the three-dimensional Gaussian profile.[16] This term is eliminated in the current analysis for simplicity but can be reconsidered easily whenever needed.

It can be seen from eq 1 that the propagator, which varies for different diffusion systems, plays a key role in the FCS theoretical framework. The propagator is the solution of the diffusion equation, which is a partial differential equation of concentration, depicting this diffusion system for a point source initial condition.

For three-dimensional free translational diffusion, $C(\vec{r}) = C_0$. The differential equation is

$$\frac{\partial C(\vec{r},t)}{\partial t} = D\nabla^2 C(\vec{r},t) \tag{3}$$

where D is the diffusion coefficient. The propagator is

$$P(\vec{r},\vec{r}',\tau) = (4\pi D\tau)^{-3/2} \exp\left[-\frac{(\vec{r}-\vec{r}')^2}{4D\tau}\right] \tag{4}$$

which leads to an analytical expression of the autocorrelation function

$$G(\tau) = \frac{1}{N}\left[1+\frac{\tau}{\tau_D}\right]^{-1}\left[1+\frac{\tau}{k^2\tau_D}\right]^{-1/2} \tag{5}$$

where $k = z_0/w_0$, $N = C_0V$, $V = \pi^{3/2}w_0^2 z_0$ is the focal volume, and $\tau_D = w_0^2/4D$ is the diffusion time, which measures the average time it takes for a particle to diffuse through the focal volume.

In the presence of a force field by a potential $U(\vec{r})$, diffusion is described by the Smoluchowski equation[17]

$$\frac{\partial C(\vec{r},t)}{\partial t} = D\nabla\left[\nabla C(\vec{r},t) + \frac{\nabla U(\vec{r})}{k_B T} C(\vec{r},t)\right] \tag{6}$$

where k_B and T are Boltzmann's constant and Kelvin temperature, respectively.

The gradient potential due to a focused laser beam of Gaussian profile is[6]

$$U(\vec{r}) = -\frac{\alpha}{2}E^2(\vec{r}) = -\frac{\alpha P W(\vec{r})}{\pi\epsilon_0 c n_m {w_0}^2} \tag{7}$$

where α, $E(\vec{r})$, P, n_m, c, and ϵ_0 represent the polarizability of the particles, the electrical field strength of the laser, the laser power, the refractive index of the medium, the speed of light, and the dielectric constant of vacuum, respectively.

Equilibrium concentration can be calculated from the Smoluchowski equation or the Boltzmann distribution

$$C(\vec{r}) = C_0\, e^{-U(\vec{r})/k_B T} = C_0\, e^{\theta W(\vec{r})} \tag{8}$$

where

$$\theta = \alpha P/\pi\epsilon_0 c n_m {w_0}^2 k_B T = U(0)/k_B T \tag{9}$$

is a dimensionless factor that measures the peak strength of the gradient field relative to the thermal energy.

If we can derive the propagator by solving the Smoluchowski equation for point source initial conditions, then the autocorrelation function can be obtained directly by either analytical or numerical approaches. However, solving such a multidimensional problem with sufficient precision is computationally intensive. Therefore, it is not practical to calculate and fit the FCS curves using a personal computer. The problem can be simplified if spherical symmetry exists, i.e., $w_0 = z_0$ and $k = 1$. Then r can be used in instead of $\vec{r}$ to reduce the problem to a one-dimensional one. In fact, a symmetrical system does exist in two-dimensional applications, such as FCS measurements on cellular membranes.[5] For three-dimensional applications, k is a geometry factor characterizing the shape of the detection volume defined by the focal spot and the confocal pinhole. In real experiments, k usually ranges from 2 to 5, indicating a prolate spheroid profile. By setting $k = 1$, the detection volume is assumed to be spherical. Although such a condition cannot be achieved in real experiments, it will be shown in this work that errors in the fitted parameters are systematic and can be eliminated by ratiometric measurements that are widely used in single-molecule experiments.[18,19]

3. Calculations and Tests

For $k = 1$, a "radial concentration" $C(r,t)$ can be defined that reduces the equation to a one-dimensional one. The particle number in the spherical shell of radius r and thickness dr is

$$C(r,t)\,\mathrm{d}r = C(\vec{r},t)4\pi r^2\,\mathrm{d}r \tag{10}$$

$C(r, t)$ satisfies the "radial" Smoluchowski equation

$$\frac{\partial C(r,t)}{\partial t} = D\frac{\partial}{\partial r}\left[\frac{\partial C(r,t)}{\partial r} - 2\frac{C(r,t)}{r} - \theta\frac{\partial W(r)}{\partial r}C(r,t)\right] \tag{11}$$

Equation 11 can be solved numerically for the initial condition of a δ function $P(r,r',0) = \delta(r - r')$ to get the "radial propagator" $P(r,r',\tau)$. Then the autocorrelation function is calculated as

$$G(\tau) = \frac{\int\int W(r)\, e^{\theta W(r)} P(r,r',\tau) W(r') 4\pi r^2\,\mathrm{d}r\,\mathrm{d}r'}{C_0[\int W(r)\, e^{\theta W(r)} 4\pi r^2\,\mathrm{d}r]^2} \tag{12}$$

Similar results can be derived for two-dimensional systems

$$C(r,t)\,\mathrm{d}r = C(\vec{r},t)2\pi r\,\mathrm{d}r \tag{13}$$

$$\frac{\partial C(r,t)}{\partial t} = D\frac{\partial}{\partial r}\left[\frac{\partial C(r,t)}{\partial r} - \frac{C(r,t)}{r} - \theta\frac{\partial W(r)}{\partial r}C(r,t)\right] \tag{14}$$

$$G(\tau) = \frac{\int\int W(r)\, e^{\theta W(r)} P(r,r',\tau) W(r') 2\pi r\,\mathrm{d}r\,\mathrm{d}r'}{C_0[\int W(r)\, e^{\theta W(r)} 2\pi r\,\mathrm{d}r]^2} \tag{15}$$

MATLAB was used for the calculations. Through the use of the "PDEPE" routine, the radial Smoluchowski equation (eq 11 or 14) was solved numerically to obtain the radial propagator $P(r,r',\tau)$. r was sampled at a mesh of ranges r_{max} and span dr. It was found that good results were obtained at $r_{max} = 12w_0$ and d$r = 0.1w_0$ (Figure 1). When calculating the FCS curves using eq 12 or 15, a direct sum rather than integration was used to reduce the computation time without apparent loss in precision. A curve can be calculated in seconds on a personal computer.

The fits were carried out using the "LSQCURVEFIT" routine in the "Optimization Toolbox" of MATLAB. This function does not require the calculation of the Jacobian of the model function,

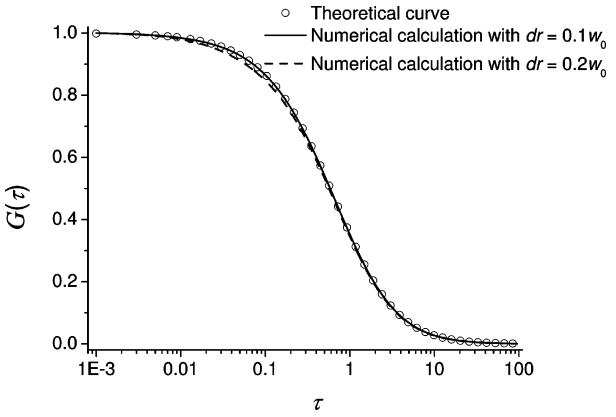

Figure 1. Comparison of calculated FCS curves to a theoretical prediction by eq 5 with $k = 1$. The two curves were calculated with $r_{max} = 12w_0$ and d$r = 0.1w_0$ and d$r = 0.2w_0$, respectively. We can see that the d$r = 0.1w_0$ results are in very good agreement with the theoretical prediction.

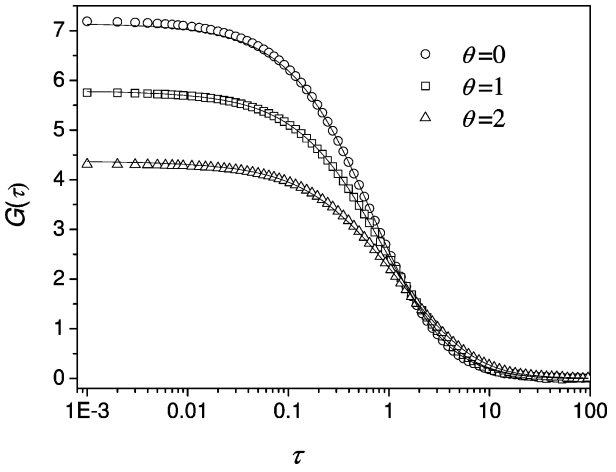

Figure 2. Fittings of simulated FCS spectra to calculated curves by the numerical approach. The spectra were simulated for spherical systems with different θ values. Spectra simulated for two-dimensional systems (not shown) gave familiar results.

TABLE 1: Fitted Parameters from Simulated FCS Spectra for Three-Dimensional Spherical Symmetrical Systems and Two-Dimensional Circular Symmetrical Systems with Different Gradient Potentials[a]

	fitted parameters					
	3D system			2D system		
θ set	N	τ_D	θ	N	τ_D	θ
0.0	0.140	1.026	0.009	0.172	0.989	0.000
0.5	0.137	0.995	0.500	0.178	0.993	0.500
1.0	0.141	0.996	1.000	0.177	0.990	1.000
1.5	0.138	1.000	1.500	0.172	0.984	1.500
2.0	0.138	1.001	2.000	0.169	1.008	2.000

[a] The parameters set in the program, except θ as given in the table, are $N = 0.13921$ and $\tau_D = 1$ for 3D systems and $N = 0.17453$ and $\tau_D = 1$ for 2D systems. The total particle number is 50 for all of the simulations. The simulation region is a 30 × 30 square for the 2D simulations.

which is very difficult for us to evaluate. The optimization parameter TolX $= 10^{-4}$ is set when calling the "LSQCURVEFIT" routine to restrict the termination tolerance on the fitted parameters.

Experiments must be carefully designed for quantitative analysis of biased FCS measurements. For a two-laser scheme,[10,12] in which one weak laser is used to excite the fluorescent molecules and another intense IR laser is used to generate the

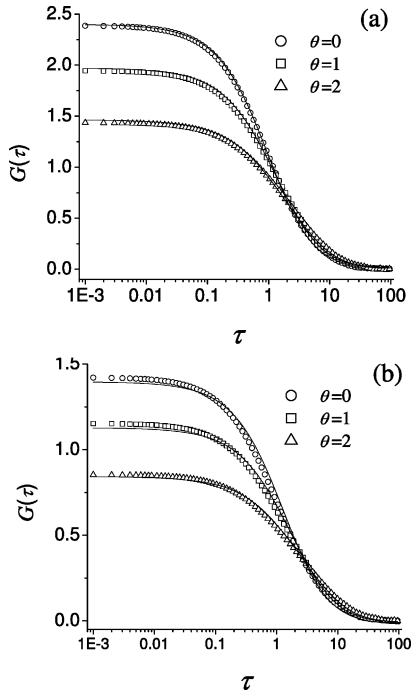

Figure 3. Fittings of simulated FCS spectra. Curves a and b are fitted for $k = 3$ and $k = 5$ systems, respectively, with different θ values.

TABLE 2: Fitted Parameters from Simulated FCS Spectra for Nonspherical Symmetrical Systems with Different Gradient Potentials[a]

	fitted parameters					
	$k = 2$			$k = 3$		
θ set	N	τ_D	θ	N	τ_D	θ
0.0	0.559	1.350	0.000	0.418	1.491	−0.000
0.5	0.563	1.385	0.500	0.414	1.465	0.500
1.0	0.568	1.374	1.000	0.416	1.514	1.000
1.5	0.556	1.385	1.500	0.416	1.506	1.500
2.0	0.548	1.368	2.000	0.415	1.533	2.000
	$k = 4$			$k = 5$		
	N	τ_D	θ	N	τ_D	θ
0.0	1.134	1.588	0.000	0.706	1.979	−0.000
0.5	1.112	1.618	0.500	0.707	1.970	0.500
1.0	1.110	1.645	1.000	0.716	1.958	1.000
1.5	1.116	1.624	1.500	0.704	1.974	1.500
2.0	1.091	1.725	2.000	0.710	1.993	2.000

[a] The parameters set in the program are $\tau_D = 1$, $N = 0.5568$, 0.4176, 1.1137, and 0.69605 for $k = 2$, 3, 4, and 5 systems, respectively. The total particle number was 50 for the $k = 3$ and 5 simulations and 100 for the $k = 2$ and 4 simulations.

gradient field, overlap of the two laser focal spots directly affects the recorded data. Extra caution has to be taken to ensure that the two focal spots coincide and have matching sizes and shapes. For a single-laser scheme, in which an intense laser generates both the fluorescence and the gradient field, effects due to excitation saturation[20−22] and photobleaching[23] may have to be considered as the gradient field strength increases. Previous experiments with such schemes showed that diffusion times increased linearly with excitation intensity for R6G molecules.[11,13] However, the trend was much faster for microspheres.[12,13] More detailed theoretical analysis and simulated FCS spectra also verified that the trend of diffusion times should be faster than a linear growth.[14] Experiments on microspheres should have revealed more about the effects of laser gradient field, since they suffer less from the interferences of excitation

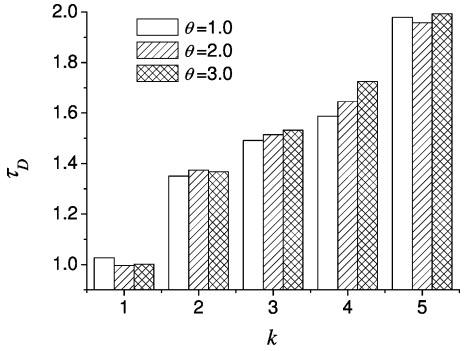

Figure 4. Fitted diffusion time τ_D vs k. τ_D value set in the simulation program is 1.0. The larger deviation of the system from spherical symmetry (larger k values) leads to larger diffusion times, whereas gradient potential has no evident effects.

saturation, which was proven to be of a considerable effect on R6G measurements.[13] Therefore, the microspheres seem to be a better system for the validation of the theoretical analysis of biased FCS. Moreover, polarizability of the microspheres can be controlled by varying their sizes and can become orders of magnitude higher than that of R6G molecules. Therefore, the effects of the gradient field are much more prominent for microspheres.

In this work, the numerical approach is tested using data generated by a Monte Carlo simulation program rather than data from experiments. This program allows us to examine separately effects due to different experimental factors, which are usually entangled in real experiments. The reliability of the simulations has been tested in previous studies.[14,21]

Simulation of the gradient field is based on the following analysis.[14] If the step time of the simulation is small enough so that the gradient force during each step is approximately constant, then an analytical solution of the Smoluchowski equation (eq 6) is available

$$P(\vec{r},\vec{r}_0,\tau) = (4\pi D\tau)^{-3/2} \exp\left[-\frac{\left(\vec{r} - \vec{r}_0 - \frac{D\vec{F}}{k_B T}\tau\right)^2}{4D\tau}\right] \quad (16)$$

Equation 16 indicates that the displacement of particle i during each simulation step T_s is

$$\vec{r^i} = \vec{r_0^i} + \frac{D\vec{F}}{k_B T}T_s + R^i \quad (17)$$

where R^i is a random vector following a normal distribution

$$\langle R^i \rangle = 0, \langle R^i R^j \rangle = \delta_{ij} 2DT_s \quad (18)$$

For simplicity, we only consider translational diffusion dynamics of small independent particles and neglect interactions among them. If we choose $w_0 = 1$ and $\tau_D = 1$, then the problem becomes dimensionless. Only θ is set in the program instead of all the other parameters in eq 9. The simulation region is a $10 \times 10 \times 10$ cube, and the focal spot of the excitation laser beam is positioned at its center. Between 50 and 100 particles are placed randomly in the cube at the initial time for different concentrations, then they undergo a random walk according to eq 17 with simulation step $T_s = 0.001$. During the simulation, periodic boundary conditions are assumed to keep the concentration constant. Since the fluorescence intensity does not appear in the normalized FCS formula, the fluorescence contribution from each particle is calculated during each step with an arbitrary unit. In the simulation, 10^7 steps are iterated before the program stops. Correlation functions are then calculated using a symmetric normalization scheme to reduce the effect of the boundary conditions on the variance of the correlation function at large lag times.[24,25] To reduce fluctuations, the final FCS curve is the average of 10 repeated simulations.

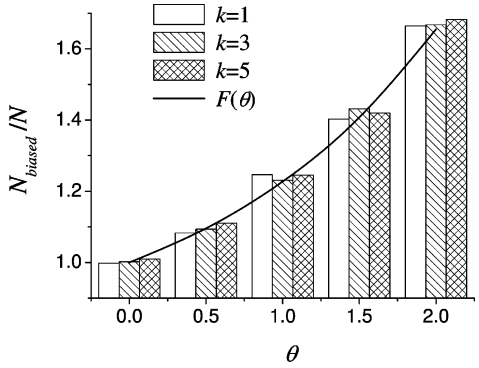

Figure 5. Biased local concentration compared to $F(\theta)$. We use the reciprocal of $G(0)$ of simulated FCS curves as an indication of biased particle number, N_{biased}. Theoretically, it can be calculated by the $F(\theta)$ function in eq 21, as is also shown in the figure.

4. Results

Simulated FCS spectra for spherically symmetrical ($k = 1$) systems were fitted using this numerical approach. The results are shown in Figure 2 and Table 1.

We can see from Figure 2 that simulated spectra can fit well to FCS curves calculated by this approach. From the fittings, we obtain N, the particle number in the focal volume, and τ_D, the diffusion time, as well as θ, which is proportional to the product of laser intensity and the polarizability of particles, α. The maximum of the relative errors in the retrieved parameters is around 3%. N and τ_D retrieved by this approach are unbiased values unaffected by the laser gradient field. They are independent of θ. Unbiased parameters are of more interest since they can be used to calculate the macroscopic concentration C_0 of the solution and the diffusion coefficient D of the particles directly.

Though this approach is derived for spherical systems, we attempted to apply it to systems of ellipsoidal symmetry, as in real experiments. The results are shown in Figure 3 and Table 2.

Figure 3 shows that the discrepancy between the simulated data and the fitted curve becomes more apparent as k increases. The systematic errors in fitted parameters N and τ_D are shown in Table 2. A larger k value results in slightly larger N values ($<3\%$ for $k = 5$) and significantly larger τ_D values (almost 100% for $k = 5$). No evident systematic errors are shown in the fitted θ values. It is important to point out that though the deviations in N and τ_D increase with k, they are independent of the gradient field. Almost the same parameters are obtained for all θ values. Figure 4 shows the trend of the fitted diffusion times versus k for three field strengths.

5. Conclusion and Discussion

When intense enough, a laser gradient field can alter the diffusion dynamics and lead to a higher local concentration around the focal spot and a longer diffusion time across the focal volume. As a result, both the shape and the interception of the FCS curves are changed. N and τ_D obtained by fitting these curves to the field-free FCS formula increase with the laser intensity.[14] In this work, using the "spherical symmetry" assumption, we can apply a numerical approach to calculate

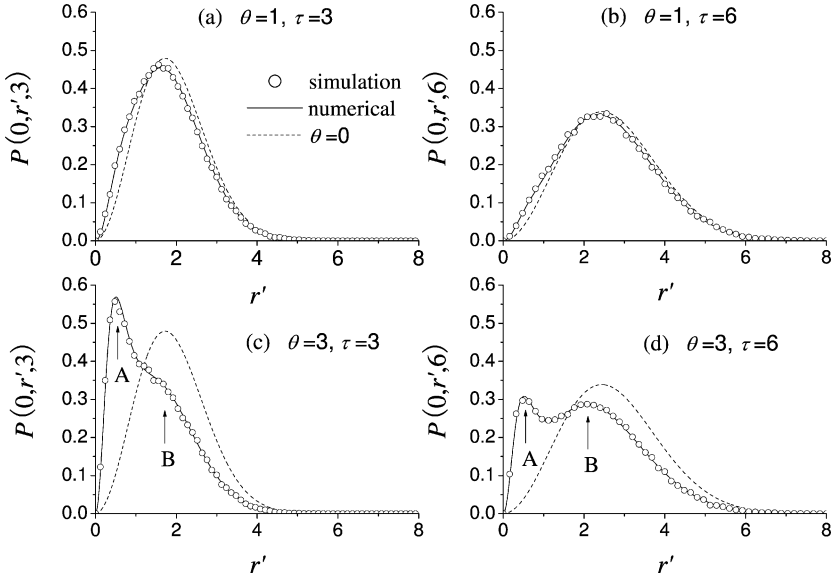

Figure 6. Comparison of propagators simulated and calculated. Propagators a and b are at $\tau = 3\tau_D$ and $\tau = 6\tau_D$ respectively, with $\theta = 1$. Propagators c and d are with $\theta = 3$. Propagators for $\theta = 0$ are also shown for comparison.

and fit the biased FCS curves directly. From the fittings, we obtain not only the unbiased N and τ_D but also θ and α. θ measures the interaction between the sample molecules and the gradient field. α is the polarizability of the sample molecules and is a sensitive indicator of the electronic structure of the molecule and the local microenvironment. For example, a folding protein has a higher polarizability than a folded protein due to the changes in the electron distribution.

Though spherical symmetry does not represent the real experimental conditions, the good agreements between the simulated data and the fitted curves prove that this approach is sufficient to describe the major effects due to the gradient potential. For systems such as a cellular membrane, circular symmetry does exist. Therefore, this approach can be directly applied without further extension.

For real experimental setups where $k > 1$, this approximation will introduce systematic errors in the fitted parameters. The magnitude of the errors increase as k increases but is independent of θ and hence the type of sample molecules. Therefore, these errors can be corrected by a standard calibration procedure, such as using a reference sample with known parameters as we do in normal FCS measurements. The calibration procedure will also eliminate other factors contained in θ, such as laser power and reflectivity of mirrors, to retrieve exact α values.

5.1. Local Concentration. It has been shown that N is much less sensitive to k. This is because k describes the shape of the focal spot rather than its size. The misuse of k only changes the shape of the FCS curves, not the interception at $\tau = 0$, as can be seen in eq 5. It can be proven that this is also valid for the biased systems.

For any diffusion systems, they satisfy

$$P(\vec{r},\vec{r}_0,0) = \delta(\vec{r} - \vec{r}_0) \tag{19}$$

This leads to[14]

$$G(0) = \frac{\int W^2(\vec{r})\, e^{\theta W(\vec{r})}\, d^3\vec{r}}{C_0[\int W(\vec{r})\, e^{\theta W(\vec{r})}\, d^3\vec{r}]^2} \tag{20}$$

We can derive that

$$F(\theta) \equiv \frac{N_{biased}}{N} = \frac{1}{\sqrt{8}\left[\sum_{n=1}^{\infty} \frac{\theta^{n-1}}{n!\sqrt{n}}\right]^2 / \sum_{n=2}^{\infty} \frac{(n-1)\theta^{n-2}}{n!\sqrt{n}}} \tag{21}$$

where $N_{biased} = 1/G(0)$ is the biased particle number in the focal spot. Equation 21 shows that the local concentration does not depend on k, only on θ. This result is tested by simulated data as shown in Figure 5.

Figure 5 shows that the biased local concentration increases with the laser gradient field as predicted by eq 21. We can see a 20%−25% difference between N and N_{biased} when the gradient potential is comparable to the thermal energy. As the laser power increases, N_{biased} can be much larger than N. Figure 5 also verifies that N_{biased} is independent of k, which explains the reason misuse of k does not introduce large error in N.

5.2. Diffusion Mobility. τ_D conceals the effect of the geometry of the focal volume. In fact, three characteristic times should be defined instead of τ_D alone; $\tau_x = \tau_y = \tau_D$ and $\tau_z = k^2\tau_D$, where τ_x, τ_y, and τ_z represent diffusion times along the x, y, and z axes, respectively. Thus, the expression of the autocorrelation function can be rewritten as

$$G(\tau) = \frac{1}{N}\left[1 + \frac{\tau}{\tau_x}\right]^{-1/2}\left[1 + \frac{\tau}{\tau_y}\right]^{-1/2}\left[1 + \frac{\tau}{\tau_z}\right]^{-1/2} \tag{22}$$

Therefore, contrary to N, both the occupation time of the sample molecules within the focal volume and the shape of the FCS curves are strongly dependent on the geometry factor k. For real experimental systems, the "spherical symmetry" assumption will significantly change the fitted τ_D, which as mentioned above can be eliminated by calibration.

5.3. Diffusion Distribution. The numerical approach allows one to examine the propagator directly to understand behavior of a biased diffusion. Figure 6 shows simulated and calculated propagators.

Figure 6 shows good agreements between calculation and simulation. As shown in Figure 6, parts c and d, there are two peaks in the spatial distribution of the propagator, corresponding to two mechanisms governing the diffusion behavior of the particles. Peak B represents the effects due to free diffusion. Peak A represents the effects due to the trapping gradient field. It is determined by the geometry of the gradient potential or

the focal spot of the laser beam. As time increases, peak A remains stationary at $r \approx 0.5w_0$. When the strength of the gradient force increases, the integrated area under peak A increases, which means an increasing local particle concentration due to the attractive gradient force. Peak B represents the free diffusion process of the particles. It "propagates" away from its initial position ($r = 0$) as time increases. When the strength of the gradient force increases, the diffusing particles are subject to a stronger attraction toward the center of the potential well, making peak B increasingly lag behind the peak of zero-field propagator. The relative integrated area of peak B also increases with time. Particles will finally escape the control of the gradient force.

Acknowledgment. This work was supported by the National Natural Science Foundation of China under grants 19928408, 60138010, and 10274039.

References and Notes

(1) Magde, D.; Elson, E.; Webb, W. W. *Phys. Rev. Lett.* **1972**, *29* (11), 705−708.
(2) Berland, K. M.; So, P. T. C.; Gratton, E. *Biophys. J.* **1995**, *68* (2), 694−701.
(3) Schwille, P.; Korlach, J.; Webb, W. W. *Cytometry* **1999**, *36* (3), 176−182.
(4) Schwille, P. *Cell Biochem. Biophys*. **2001**, *34* (3), 383−408.
(5) Hess, S. T.; Huang, S. H.; Heikal, A. A.; Webb, W. W. *Biochemistry* **2002**, *41* (3), 697−705.
(6) Ashkin, A.; Dziedzic, J. M.; Bjorkholm, J. E.; Chu, S. *Opt. Lett.* **1986**, *11* (5), 288−290.
(7) Ashkin, A. *Proc. Natl. Acad. Sci. U.S.A.* **1997**, *94* (10), 4853−4860.
(8) Ashkin, A. *Method Cell Biol.* **1998**, *55*, 1−27.
(9) Kuyper, C. L.; Chiu, D. T. *Appl. Spectrosc.* **2002**, *56* (11), 300A−312A.
(10) Chiu, D. T.; Zare, R. N. *J. Am. Chem. Soc.* **1996**, *118* (27), 6512−6513.
(11) Osborne, M. A.; Balasubramanian, S.; Furey, W. S.; Klenerman, D. *J. Phys. Chem. B* **1998**, *102* (17), 3160−3167.
(12) Ding, Y.; Meng, F. B.; Chen, B.; Ma, H.; Lei, J.; Chen, D. Y. *Acta Phys. Sin.* **2001**, *50* (11), 2269−2274.
(13) Chirico, G.; Fumagalli, C.; Baldini, G. *J. Phys. Chem. B* **2002**, *106* (10), 2508−2519.
(14) Meng, F. B.; Chen, B.; Liu, G.; Ma, H. *Chin. Phys. Lett.* **2004**, *21* (4), 760−763.
(15) Byron, F. W.; Fuller, R. W. *Mathematics of Classical and Quantum Physics*; Addison-Wesley: Reading, MA, 1969.
(16) Wohland, T.; Rigler, R.; Vogel, H. *Biophys. J.* **2001**, *80* (6), 2987−2999.
(17) Risken, H. *The Fokker−Planck Equation: Methods of Solution and Applications*, 2nd ed.; Springer-Verlag: New York, 1989.
(18) Dahan, M.; Deniz, A. A.; Ha, T. J.; Chemla, D. S.; Schultz, P. G.; Weiss, S. *Chem. Phys.* **1999**, *247* (1), 85−106.
(19) Deniz, A. A.; Laurence, T. A.; Dahan, M.; Chemla, D. S.; Schultz, P. G.; Weiss, S. *Annu. Rev. Phys. Chem.* **2001**, *52*, 233−253.
(20) Widengren, J.; Mets, U.; Rigler, R. *J. Phys. Chem.* **1995**, *99* (36), 13368−13379.
(21) Ding, J. Y.; Chen, B.; Meng, F. B.; Ma, H. *Acta Phys. Sin.* **2004**, *53* (8), 2503−2508.
(22) Berland, K. *Biophys. J.* **2004**, *86* (1), 334A.
(23) Eggeling, C.; Widengren, J.; Rigler, R.; Seidel, C. A. M. *Anal. Chem.* **1998**, *70* (13), 2651−2659.
(24) Schätzel, K.; Drewel, M.; Stimac, S. *J. Mod. Opt.* **1998**, *35*, 711−718.
(25) Saffarian, S.; Elson, E. *Biophys. J.* **2003**, *84* (3), 2030−2042.